HiSST: International Conference on High-Speed Vehicle Science Technology
26–29 November 2018, Moscow, Russia

Performance and Stability Analysis of a Hypersonic Vehicle for a Low Speed Flight Test Program

T. Bykerk[1], D. Verstraete[1], S. Wolf[2], V. Villace[2] and J. Steelant[2]

Abstract

Hypersonic vehicle design usually focuses on the aerodynamic, structural and thermal challenges at high speed. However, applications involving a traditional horizontal take-off and landing require the vehicle to fly from low subsonic speeds up to the design hypersonic Mach number. In preparation for a low speed flight test program, a modified scaled model of the Hexafly-International Mach 7.4 waverider has been built and tested in the University of Sydney 7x5 Low Speed Wind Tunnel to evaluate its static stability and performance. Results to date indicate that the vehicle is stable, trimmable and can cruise at a speed suitable for remote piloting. In addition, the required speed and angle of attack for take-off and landing are within acceptable limits, giving confidence in the feasibility of the proposed low speed flight test program.

Keywords: Low Speed, Stability, Performance, Waverider

Nomenclature

AoA – Angle of Attack
AoS – Angle of Sideslip
CFD – Computational Fluid Dynamics
LiPo – Lithium Polymer Battery Cell
MRC – Moment Reference Centre
S – Lithium Polymer Battery Cells in Series

1. Introduction

Hypersonic vehicles using airbreathing engines are a potential solution for civilian transport between major world cities. These aircraft are of interest on current long-haul flight routes exceeding 10 hours in duration as the travel time can be reduced considerably. The majority of research into hypersonic aircraft is confined to overcoming the challenges associated with high Mach numbers, namely aerodynamics, airframe heating, structural design, stability and propulsion systems. However, for civilian applications, the vehicles must also be able to take-off and land horizontally as well as be stable throughout the entire flight envelope. As the airframe shape is typically optimised for the design point, a sharp, slender vehicle with highly swept, low aspect ratio delta-style wings is commonplace. As a result, low speed performance and stability can be compromised but is rarely investigated. Some research and flight test programs have been conducted in the past, but the datasets are largely incomplete, generally neglecting to present quantitative results for stability derivatives.

During the late 1990's Accurate Automation Corporation (AAC) worked with NASA and undertook the LoFLYTE™ program, where the low speed flight regime of an optimised Mach 5.5 waverider was investigated [1]. Overall conclusions were that the low speed performance and handling of LoFLYTE™ were satisfactory and calculated take-off and landing speeds were plausible. Strong leading edge vortices were observed during laser light sheet flow visualisation, with improved lifting characteristics as a result. This did result in a minor pitch up tendency, which increased in severity with AoA, highlighting potential stability issues for these types of aircraft. Leading edge flow separation and subsequent vortex formation improve lift, but vortex breakdown with increasing AoA has been shown to result in a non-linear, destabilising pitching moment [2, 3].

[1] *School of Aerospace, Mechanical and Mechatronic Engineering, Building J07, Maze Crescent, Darlington Campus, University of Sydney, NSW 2006, Australia, tamas.bykerk@sydney.edu.au, dries.verstraete@sydney.edu.au*
[2] *ESA-ESTEC, Aerothermodynamics and Propulsion Analysis Section TEC-MPA, P.O. Box 299, Noordwijk, Netherlands, Sebastian.Wolf@esa.int,victor.fernandez.villace@esa.int, Johan.Steelant@esa.int*

The only program thus far to complete both low and high speed flight tests was the X-43A, which successfully undertook Scramjet powered flight up to Mach 9.68 [4]. A low speed variant was tested by AAC [5] and was called the X-43A-LS. It was an unmanned aerial vehicle, remotely piloted from the ground. The aircraft shape from the high speed configuration underwent some modifications for the LS version. The wings and fins were enlarged and the centre of gravity shifted [6]. The investigation concluded that the aircraft was stable both longitudinally and laterally, but provided little quantitative data [5,6]. This highlighted a need to compromise in geometry between high and low speed versions.

The aim of the proposed flight test program is to build a complete picture of the low speed performance and handling qualities of a hypersonic vehicle. This work is supported by CFD and wind tunnel tests and the results from these two sections of the project are presented in this paper.

2. Hexafly International Vehicle

The Hexafly-International vehicle is the product of a research cooperation between various commercial and research institutions around the world. The aim of the project is to demonstrate the viability of civilian hypersonic transport. The vehicle is designed to cruise at a Mach number between 7 and 8 and is equipped with an internal scramjet engine shown in Fig. 1. A highly swept delta planform with anhedral allows the conical shockwave to be contained by the leading edges at the design point. One element of this project is to demonstrate the viability of take-off and landing as well as subsonic stability.

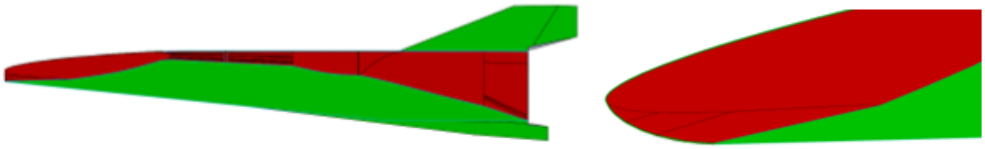

Fig 1. Hexafly-International Vehicle with Modified Internal Flow Path and Intake Lip

The low speed variant to be used for flight testing has been scaled to a length of 1.15m. Thus, the vehicle is large enough to be visible for the ground-based pilot but at the same time it is small enough to be installed in the wind tunnel. As a propulsive system, an electric ducted fan with a diameter of 90mm is used in combination with a battery consisting of eight Lithium Polymer cells connect serially. In order to integrate the electric ducted fan, additional modifications have been made to the internal flow path. The vehicle now features an S-bend duct with the lower lip of the intake rounded (5mm radius) to delay flow separation at high AoA. A contracting nozzle has replaced the divergent scramjet nozzle. These modifications are shown in Fig. 2.

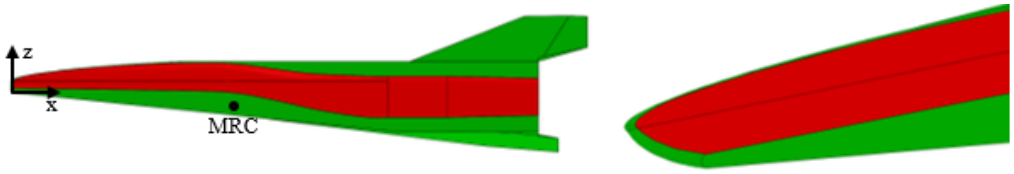

Fig 2. Hexafly-International Vehicle with Modified Internal Flow Path and Intake Lip

The mass and MRC location are based on a computer mock-up of the proposed vehicle shown in Fig. 3. The flight vehicle will be composed of a plywood frame filled with lightweight RC flight foam. For extra strength and resistance to damage, the vehicle will be covered with fibreglass and a thin coat of resin. All parts of the aircraft are modelled with the correct mass and material density to give an accurate approximation of the mass and MRC location.

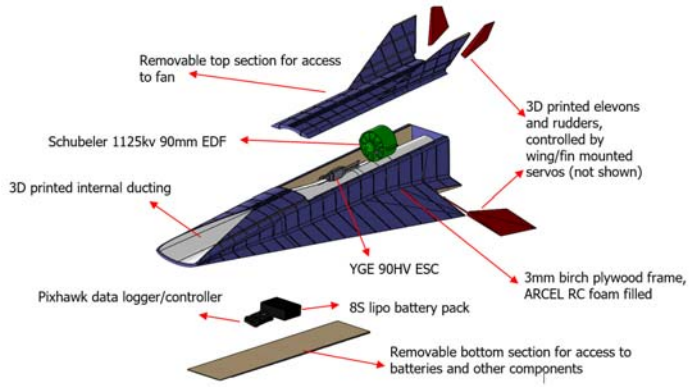

Fig 3. Exploded View of Proposed Flying Vehicle (small components not shown)

Table 1 gives an overview of the estimated properties of the flight vehicle. The location of the MRC is in the body reference frame measured from the leading edge of the inlet as shown above in Fig. 2.

Table 1. Estimated Physical Properties of Low Speed Hexafly International Test Vehicle

Property	Value	Units
Vehicle Mass	2	kg
MRC (x location)	0.511	m
MRC (y location)	0	m
MRC (z location)	-0.007	m
Reference Area	0.406	m^2
Reference Chord Length	1.15	m
Reference Span Length	0.495	m

Vehicle aerodynamics is provided according to the ISO-1151 standard, with the reference system for the aerodynamic data in a body-fixed axis system, as shown in Fig. 4. Lift and drag are presented in the wind axis system as components of C_N and C_A according to the AoA.

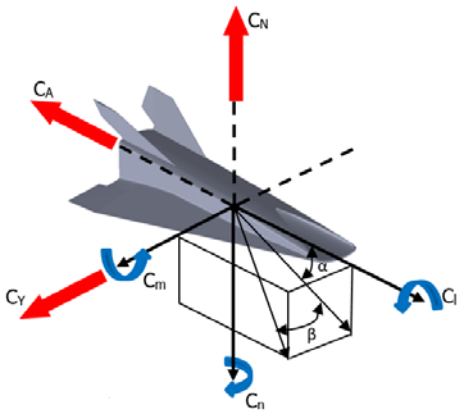

Fig 4. Body Axis Reference Frame According to ISO-1151 Standard

3. Methodology

3.1. Low Speed Wind Tunnel Testing

A full scale wind tunnel model was fabricated using an assembly of 3D printed pieces which were then glued together and sanded for a smooth finish. Components such as the elevons and rudders were

removable to allow the testing of various control settings. Fig. 5 shows the model mounted in the wind tunnel. The model was attached to a 6 component load cell taking force and moment measurements Due to the large internal duct structure, the load cell could not be recessed into the body of the model.

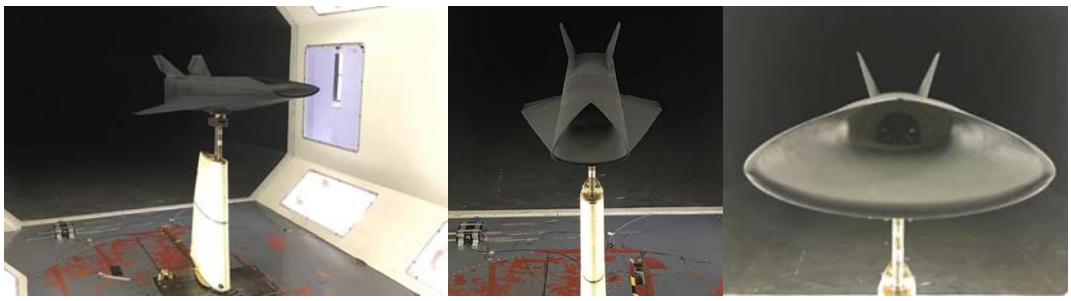

Fig 5. Views of Vehicle in Wind Tunnel

The test matrix comprised of approximately 200 tests. The data acquired during testing was from load cell data to find aerodynamic and static stability coefficients, pressure data to characterise the internal flow path and tuft flow visualisation to determine the lip flow separation tendencies. A summary of key parameters varied during the campaign are summarised in Table 2. Tests were conducted both with and without the fan installed to analyse its effects.

Table 2. Summary of Wind Tunnel Test Variables

Variable	Range	Description
AoA	-5 to 25 deg	AoA sweep for aerodynamic/pitching moment analysis. Note: at high speeds range is -5 to 15 for load cell limit. Pressure and tuft flow visualization for inlet flow quality/lip separation.
AoS	-10 to 10 deg	AoS sweep for lateral/directional static stability (variations in roll/side force and yaw due to sideslip). Pressure and tuft flow visualization for inlet flow quality/lip separation.
V_∞	0-25 m/s	Variation of flight speed for thrust loss analysis and impact of flight speed on drag.
Fan Current	15 to 25 A	Variation of fan current for different thrust settings to determine cruise thrust. Static pressure jump due from fan measured for input into CFD simulations.
d_e	-10 to 10	Variation of elevon deflections to determine longitudinal control effectiveness. Alternating for roll and yaw studies.
d_r	0 to 15 deg	Variation of rudder deflections to determine roll and yaw control.

During selected runs, total and static pressure measurements were taken to determine the nozzle jet velocity, flow quality at the fan face as well as the static pressure jump across the fan. Fig. 6 shows the locations of pressure measurement locations. Pressure tests for point 1, 2 and 3 were connected to a Scanivalve MPS-4264 digital pressure transducer unit using 0.8mm ID flexible tubing. Readings were taken at a sampling frequency of 500Hz for 5 seconds.

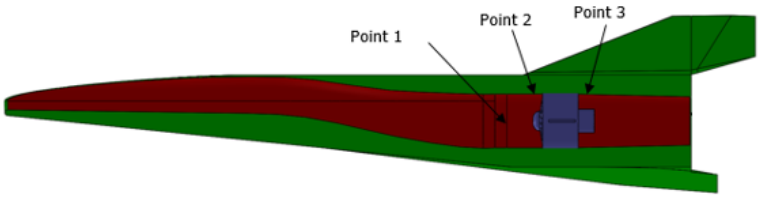

Fig 6. Locations of Pressure Measurement Points

The instrumentation at point 1 measures the fan face flow quality using total and static pressure. The cross sectional area of the duct was divided into six equal area sections. Pitot tubes were arranged central to these rings as shown in Fig. 7 (left). Pitot tubes were manufactured using 1/0.55 mm OD/ID brass tube and installed into the 3D printed duct section using a jig and the tubes were then glued in place. Fig. 7 (right) shows the final product. In total there are five rings of eight tubes, with one centrally mounted pitot. This arrangement had the best duct coverage with minimal blockage (~3.5%). Eight accompanying wall static ports (upstream of the pitots to reduce any interference) were used to calculate velocity in the duct at each point. Note that measurements at point 1 were taken individually, while the pressure jump tests with tappings at point 2 and 3 were taken simultaneously.

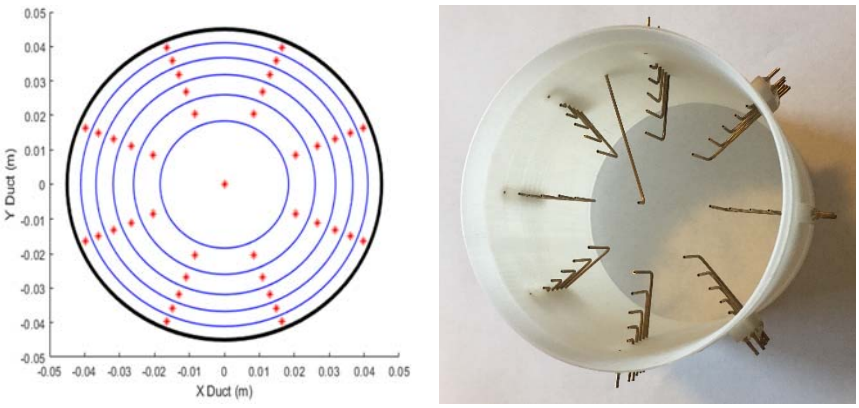

Fig 7. Point 1 Pressure Measurement Instrumentation Left: Inlet Duct Area Distribution and Right: Manufactured Duct Piece with Pitots and Static Ports Visible

Point 2 and point 3 were equipped with 10 static ports each spread equally around the circumference of the duct. These locations were chosen as it was a close to the fan as possible (without tapping the fan casing itself). Fig. 8 shows the tapped duct pieces for each location. The difference in average static pressure between the upstream and downstream fan taps was for hte CFD actuator disk model, where a pressure jump specification was required.

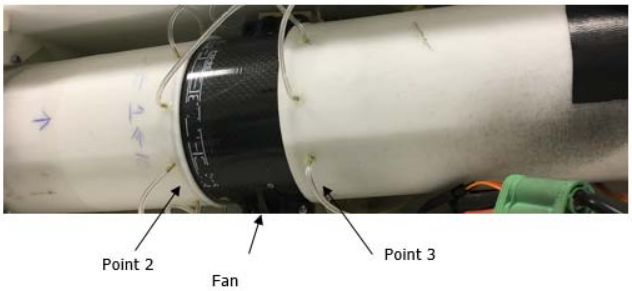

Fig 8. Point 2 and 3 Pressure Measurement Instrumentation Left: Upstream Fan Location and Right: Downstream Fan Location

Load cell measurements are only able to provide a net force during powered tests, i.e. measurements in the x body axis include both thrust and axial force as shown in Fig. 9. Depending on the fan power and configuration/angle of the vehicle, the net force can be either positive or negative.

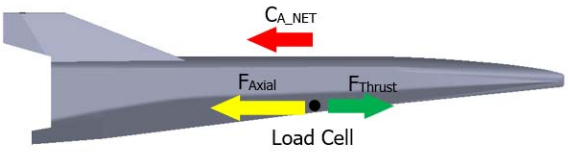

Fig 9. Net Axial Force Measured with Load Cell

To understand any flow separation tendencies at the intake lip, tuft flow visualisation was completed. Nine tufts along the lip of the inlet were arranged in three rows to determine the severity of flow separation. This qualitative analysis was used in conjunction with the pressure data to build a complete picture of this unique inlet.

3.2. CFD Simulations

The CFD component of the analysis had two purposes, firstly it was used to build confidence in modelling electric ducted fan systems using the actuator disk method and secondly, to visualise flow features not able to be seen in the wind tunnel tests. Not all tests completed in the wind tunnel component of this study (see Table 2) were replicated in CFD.

The CAD geometry for the powered simulations and mesh setup is shown in Fig. 10. The mesh comprised of unstructured tetrahedral elements with a body of influence surrounding the vehicle. A prism inflation layer has been used to capture the wall effects. The farfield extended 45 lengths upstream and 75 downstream. For longitudinal tests, a half body mesh with approximately $15x10^6$ was used to reduce computation time. The simulations were run using the k-ω SST turbulence model. For lateral simulations, a full body domain was meshed. A surface within the intake duct models the fan as an actuator disk. As previously stated, the pressure jump specification for this model was measured in the wind tunnel and applied as a boundary condition. To more accurately model the fan, the body of the motor as well as the nosecone was also included in the geometry. For studies with the airframe only the actuator disk and fan body were removed.

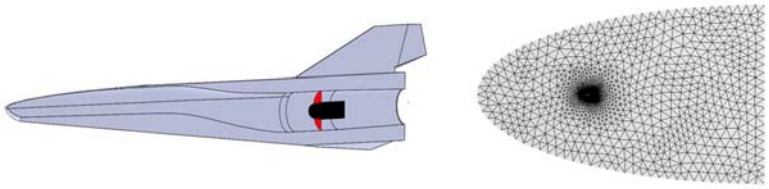

Fig 10. Left: CAD Model of Vehicle with Actuator Disk Shown in Red and Right: Farfield

4. Results

4.1. Aircraft Aerodynamics

Fig. 11 and Fig. 12 shows the lift and drag coefficients, as well as the lift to drag ratio for a full AoA sweep between -4 and 26 degrees AoA with the airframe only (fan not installed). A small non-linearity in lift is observable at approximately 0 degrees AoA, where the slope increases. This is a typical characteristic of sharp, highly swept wings and is due to leading edge flow separation causing vortex lift. Above 21 degrees AoA the gradient begins to plateau, but no clear stall is observed. A take-off speed of 15 m/s is calculated assuming the aircraft will rotate to 10 degrees AoA. The landing speed could be lowered further to 12.5 m/s if an AoA of 15 is considered.

The zero lift drag and maximum lift to drag ratio for this vehicle is observed to be significantly higher than a typical civilian aircraft (generally in the range of 0.02 [7]). This can be attributed to the shape of the aircraft (similar to a bluff body) and also the external mount with adapter plate which was required to attach the model to the load cell. The surface roughness of the model could also not be quantified and may also play a role.

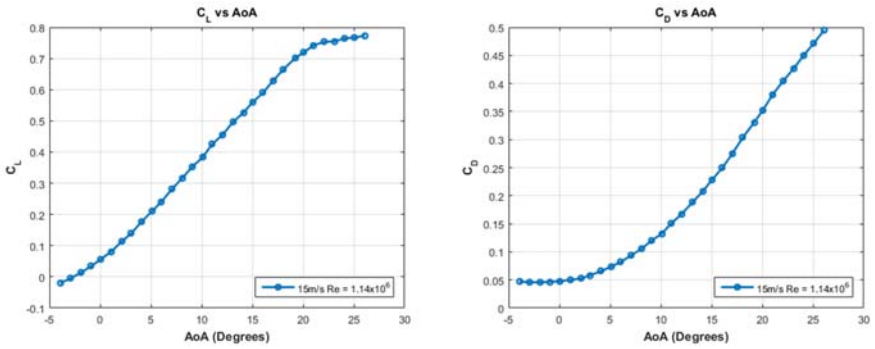

Fig 11. Left: Lift and Right: Drag Coefficient for Airframe Only at 15m/s, Re = 1.14×10^6

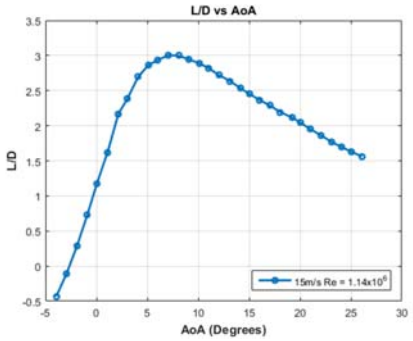

Fig 12. Lift to Drag Ratio of Airframe Only at 15m/s, Re = 1.14×10^6

Post processed images of the vehicle at various AoA from the CFD simulations are shown in Fig. 13. The growing strength of the leading edge vortices is clearly seen and confirm the lift curve slope trend seen in the wind tunnel. Surface pressure contours show increasing upper surface suction and vorticity magnitude increasing with AoA.

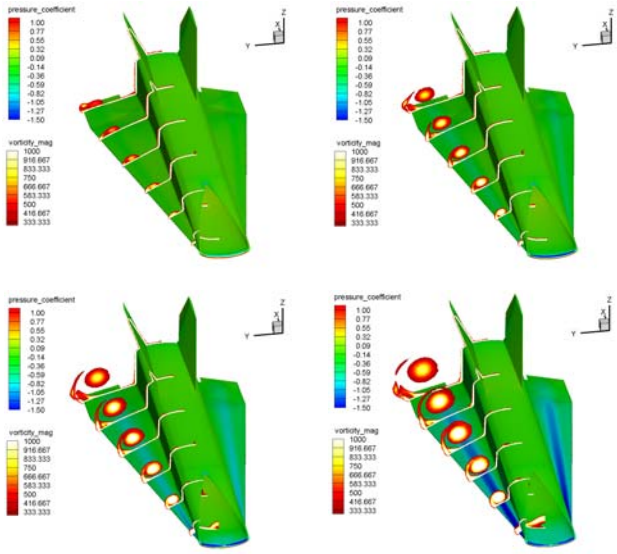

Fig 13. Vortex Visualisation from CFD at Top Left: 0, Top Right: 5, Bottom Right: 10 and Bottom Left: 15 degrees AoA for Airframe Only at 15m/s, Re = 1.14×10^6

4.2. Propulsion System Performance

The selected fan has a maximum usable voltage of 44.4V (12S). In previous tests not covered in this paper, it was deemed that the 12S and 10S configurations did not give enough throttle control (cruise power was achieved at a low current). For this reason, an 8S Lipo configuration was selected.

When an aircraft is at an AoA other than 0, there is some contribution to lift from the thrust vector. The variation in lift due to thrust is shown in Fig. 14 for the anticipated flight speed range. As forward airspeed increases, a drop in the impact of thrust on lift is seen as the fan begins to spin in the free flow, otherwise known as 'wind milling'. At the cruise and take-off speeds/AoA there is no significant improvement in lifting performance seen, so for the purposes of aircraft performance analysis, the slight variations will be ignored.

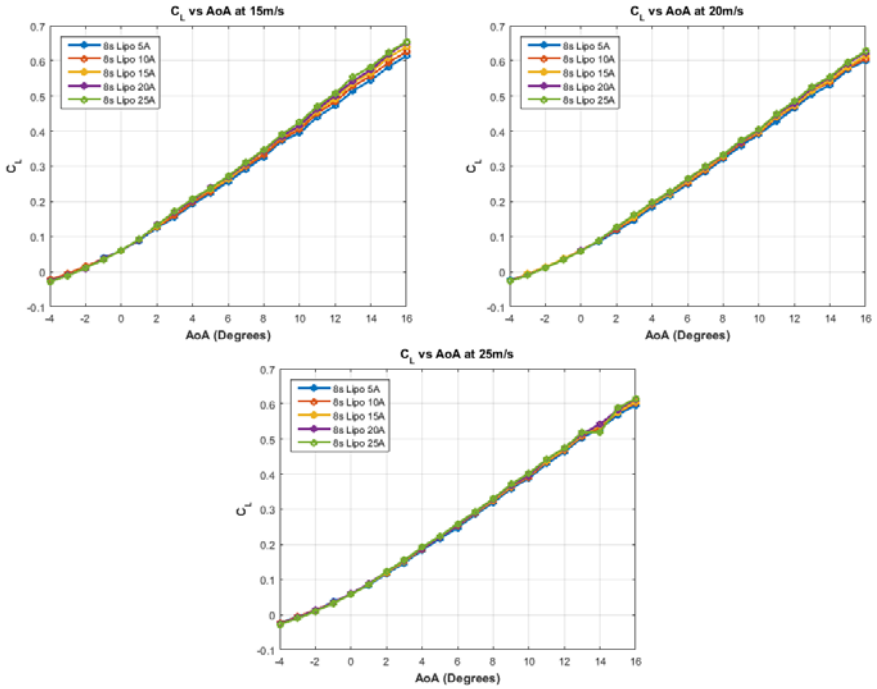

Fig 14. Lift Coefficient Increment due to Thrust for Top Left: 15m/s, Top Right: 20m/s and Bottom Centre: 25m/s

Fig. 15 shows the load cell results of drag for various power settings and forward airspeeds at the selected cruise AoA. Negative values indicate excess thrust and the positive gradient of the curves is indicative of the increasing total drag force with airspeed as well as the loss in thrust explained previously. Based on the selected cruise speed of 22m/s and using the relationship of thrust equals drag at cruise, we can estimate the required throttle setting to be 25A using 8S lipo batteries.

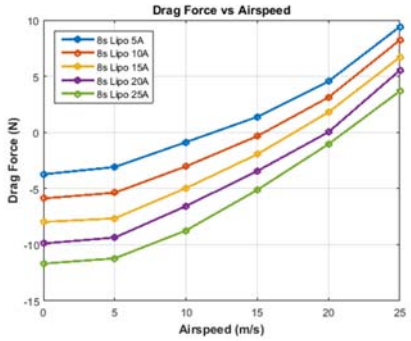

Fig 15. Total Drag Force from Load Cell vs Airspeed at 3.5 AoA

While this method allows the calculation of power setting required for cruise, it does not show the thrust developed by the fan. For the purposes of this investigation the assumption of constant drag of the airframe irrespective of thrust setting has been made.

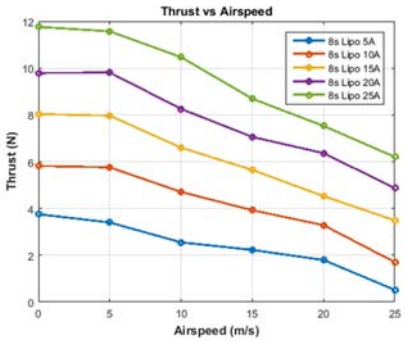

Fig 16. Thrust Estimates

Fig. 17 shows the measured static pressure jump across the fan face for varying AoA and airspeed. The pressure rise across the fan is directly related to the thrust produced and was primarily measured for input into CFD for the actuator disk boundary condition modelling the fan. The plots show minimal variance in pressure with changing AoA indicating that fan performance isn't largely affected by high incidence angles. The drop in pressure with increasing flight speed is the same phenomenon shown in previous plots.

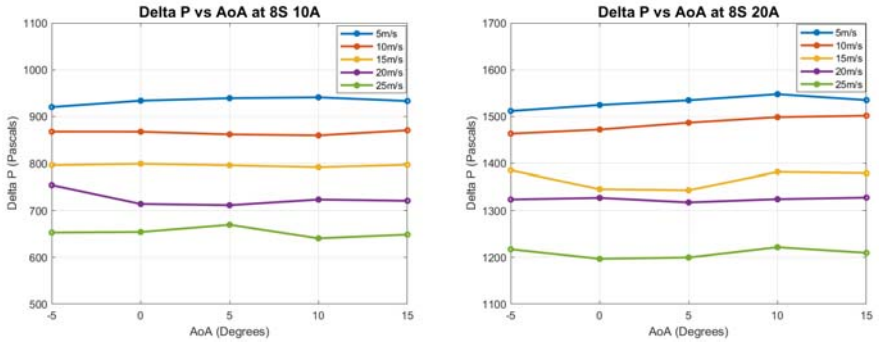

Fig 17. Left: 8S 10A and Right: 8S 20A Static Pressure Jump Across Fan

4.3. Static Stability

Static stability refers to the vehicle's tendency to return to an equilibrium point after being disturbed by a wind gust or control deflection. Curve gradients for longitudinal and lateral/directional forces and moments indicate whether the aircraft is statically stable or not. Table 3 shows a summary of the conditions which need to be met for the vehicle to be deemed statically stable.

Table 3. Static Stability Requirements [7]

Coefficient	Descriptions	Stability Type	Gradient for Stability	Stability Derivative
C_Y	Side force Coefficient	Directional	Negative	$C_{Y\beta}$
C_l	Rolling Moment Coefficient	Lateral	Negative	$C_{l\beta}$
C_m	Pitching Moment Coefficient	Longitudinal	Negative	$C_{m\alpha}$
C_N	Yawing Moment Coefficient	Directional	Positive	$C_{N\beta}$

The vehicle is found to be statically stable in pitch as seen by the negative gradient of the moment curve in Fig. 18. The exception to this is an unstable pitch break which occurs at approximately 20 degrees AoA, where the gradient switches to positive. If the vehicle was trimmed at an AoA higher than 20 degrees, the vehicle would tend to diverge from an equilibrium point. This is not concerning in this case, as the vehicle is expected to remain within the -5 to 15 degree AoA range.

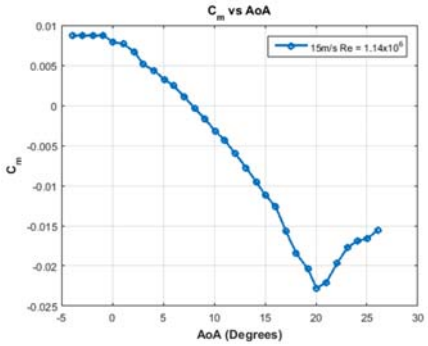

Fig 18. Pitching Moment Coefficient vs AoA of Airframe Only at 15m/s, Re = $1.14x10^6$

Fig. 19 (left) presents the side force coefficient vs AoS for -5 to 15 AoA. The gradient of each AoA case has been calculated by fitting the data linearly and is presented in Fig. 19 (right). This linear curve fit has also been applied to the rolling and yawing moment coefficients which follow. While the gradients all remain negative (showing a static stability), the gradient slope is positive meaning that increasing AoA causes a lower restoring side force. This is potentially due to the body of the vehicle progressively shielding the fins as AoA increases, hindering their ability to produce force.

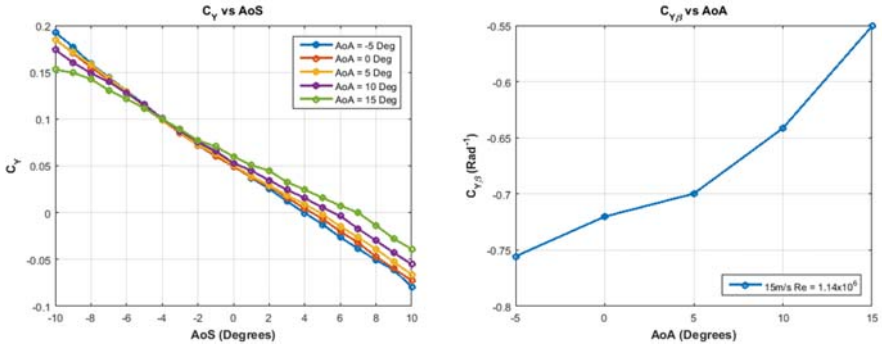

Fig 19. Left: Sideforce Coefficient vs AoS and Right: $C_{Y\beta}$ vs AoA of Airframe Only at 15m/s, Re = $1.14x10^6$

At low AoA, the gradient of the rolling moment coefficient is found to be positive, indicating static instability. Fig. 20 (right) shows that at approximately -4 degrees AoA, the gradient transitions to negative which represents a statically stable aircraft. This may play a role during descent phases and the pilot will need to be aware of the vehicle's tendency to deviate from equilibrium in roll.

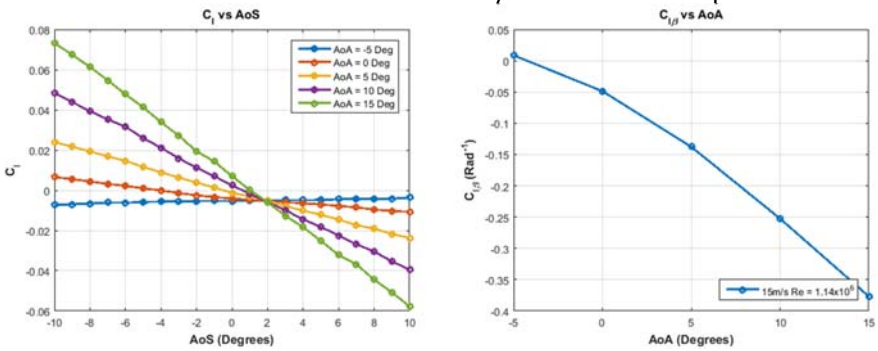

Fig 20. Left: Rolling Moment Coefficient vs AoS and Right: $C_{l\beta}$ vs AoA of Airframe Only at 15m/s, Re = $1.14x10^6$

Fig. 21 shows the results for yawing moment. For all AoAs tested, the vehicle is found to be statically stable. The restoring moment increases with AoA which is contrary to the decreasing $C_{Y\beta}$ results. This indicates that there is some wing/fuselage contribution to the yawing moment.

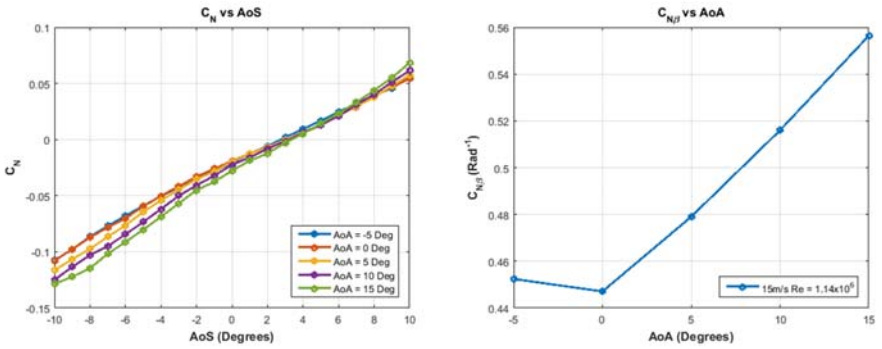

Fig 21. Left: Yawing Moment Coefficient vs AoS and Right: $C_{N\beta}$ vs AoA of Airframe Only at 15m/s, Re = $1.14x10^6$

Post processed images shown in Fig. 22 show the vortex development in sideslip conditions off the leeward side of the fin. The development of these vortices are the main contributor to fin side force development and directional stability.

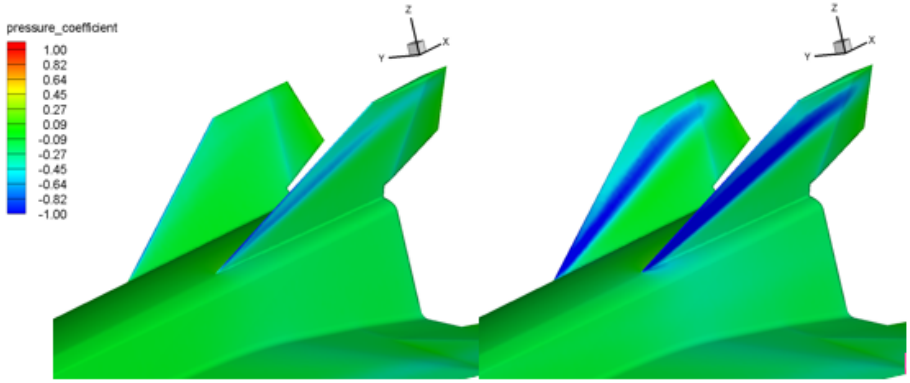

Fig 22. Fin Vortex Visualisation from CFD at Left: 0AoA and 5AoS, Right: 0AoA and 10 AoS for Airframe Only at 15m/s, Re = $1.14x10^6$

4.4. Control deflections

The control surfaces of the proposed vehicle are shown in Fig. 23, with the elevons shown in red and the rudders shown in green. For the fin sizing, there was no existing rudder sized for the unpowered glider variant, so an estimate was made according to 30% of the chord length of the fin. Elevon sizing was not required, as their dimensions were kept the same as the glider.

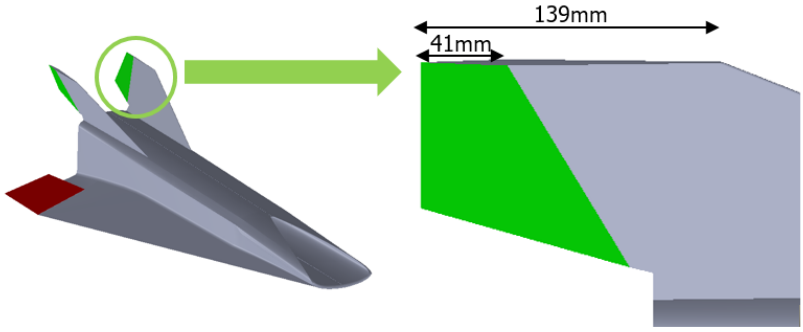

Fig 23. Control Surface Overview Left: Elevon (Red)/Rudders (Green) and Right: Rudder/Fin Dimensions

The elevon control surfaces are shown in red in the vehicle layout diagram shown in Fig. 3. Fig. 24 shows results of lift and drag for varying elevon positions. The staggered plots show that the elevons are effective in augmenting lift and follow expected trends. The maximum lift and drag coefficient is increased with downward deflections while rotating the elevons upwards will give the lower lift and drag.

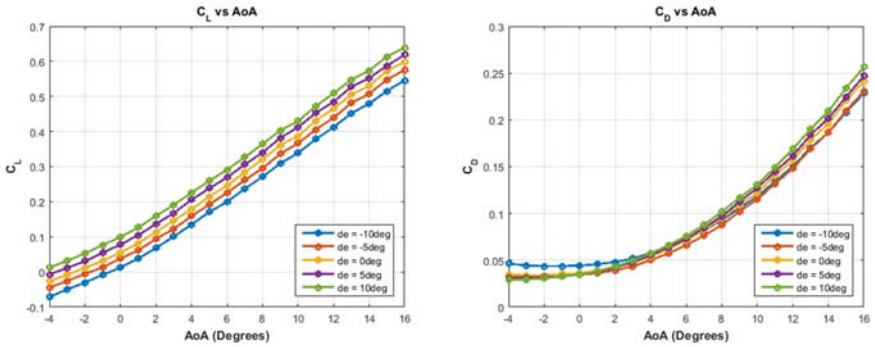

Fig 24. Left: Lift and Right: Drag Coefficient with Varying Elevon Deflections at 25m/s, Re = 1.9×10^6

Fig. 25 shows the maximum aerodynamic efficiency at 5 degrees AoA for an elevon position of 10 degrees. The maximum value of the lift to drag ratio as well as the AoA at which maximum efficiency occurs is significantly affected by elevon position. Downward deflections see higher efficiency at lower AoA while upwards deflection have a lower peak at a higher AoA. It is important to note that the lift to drag ratio for these tests is lower than shown in Fig. 11 due to Reynolds number effects.

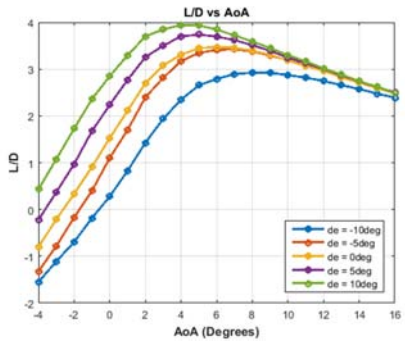

Fig 25. Lift to Drag Ratio of Varying Elevon Deflections at 25m/s, Re = 1.9×10^6

The aircraft will be easily trimmed as shown by the clearly staggered plots in Fig. 26. For the cruise configuration, an elevon setting close of approximately 4 degrees will be required.

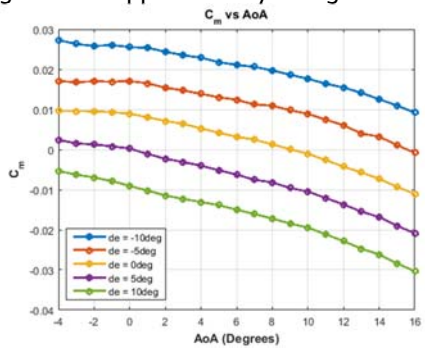

Fig 26. Pitching Moment of Varying Elevon Deflections at 25m/s, Re = 1.9×10^6

Fig. 27 shows results of asymmetric elevon deflection studies, with a positive elevon deflection on the left hand side of the vehicle. The staggered plots show control effectiveness for roll with increasing

elevon deflection. The flattening of the plots in Fig. 26 (left) at 10 de suggests that the elevons are losing control authority indicating they are close to/at their stall point. Fig. 26 (right) shows a positive rolling moment is also inducing a positive yawing moment. This shows a propensity for the aircraft to yaw into the roll and is caused by more drag caused by the upward deflected elevon compared with the downward. The magnitudes of these two plots are quite small and is due to the positioning of the elevons. Compared to traditional civilian aircraft, the ailerons are placed further outboard than on this vehicle, giving a larger roll and yaw response to deflections because of the increased moment arm.

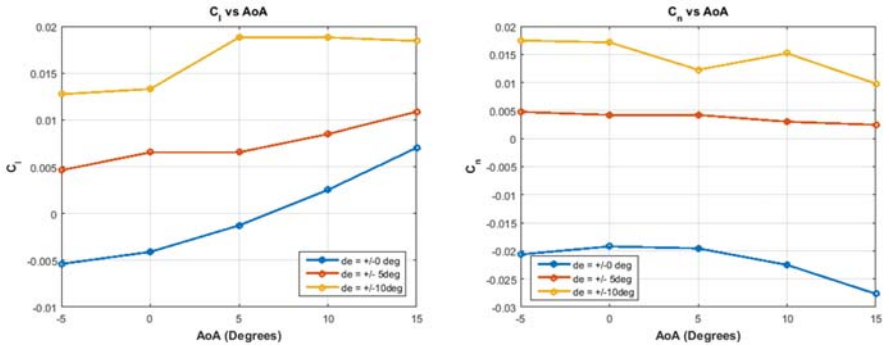

Fig 27. Left: Rolling Moment Coefficient and Right: Yawing Moment Coefficient for Asymmetric Elevon Deflections at 25m/s, Re = 1.9×10^6

Fig. 28 shows the results from negative rudder deflections on rolling and yawing moment. When considering all plots below 0 degrees AoA, the vertical separation between data points as expected. Rudder deflections induce rolling and yawing in the anticipated directions. It is clear that the rudder at 15 degrees experiences stall as shown by the sharp drop off in moment coefficient for both plots. Generally, the 5 and 10 degree deflected rudders provide better roll and yaw control with increasing AoA that the 0 degree dr case. This is potentially due to the trailing edges of the fins being better exposed to the airflow. Inspecting the magnitudes of the moment coefficients and comparing them with the asymmetric elevon deflections, we can see that the rudders are more effective for both roll and yaw control. Normally, this would be very undesirable for a regular airfraft, but in this case, where the inertia about the roll axis will be very small, less control authority will be required.

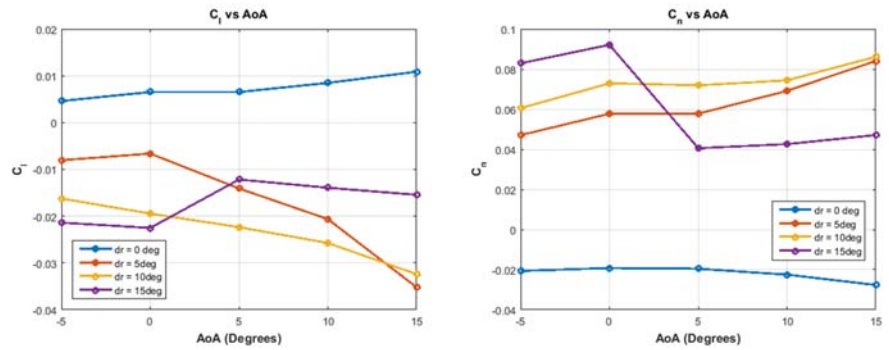

Fig 28. Left: Rolling Moment Coefficient and Right: Yawing Moment Coefficient for Rudder Deflections at 25m/s, Re = 1.9×10^6

4.5. Inlet Performance and Flow Quality

Both CFD and wind tunnel tests have confirmed the presence of a vortex originating at the top lip of the intake which is ingested by the fan. This vortex is present at all tested airspeeds and AoA, but its location varies. Figure 29 shows the CFD model for the vehicle at 0AoA and a fan setting of 20A running on 8S lipo, while Figure 13 shows the inlet x-velocity at point 1 (see Fig. 6). The wind tunnel results compare well with CFD, showing the presence of these dual vortices. This may impact the fan performance when compared with an ideal inlet.

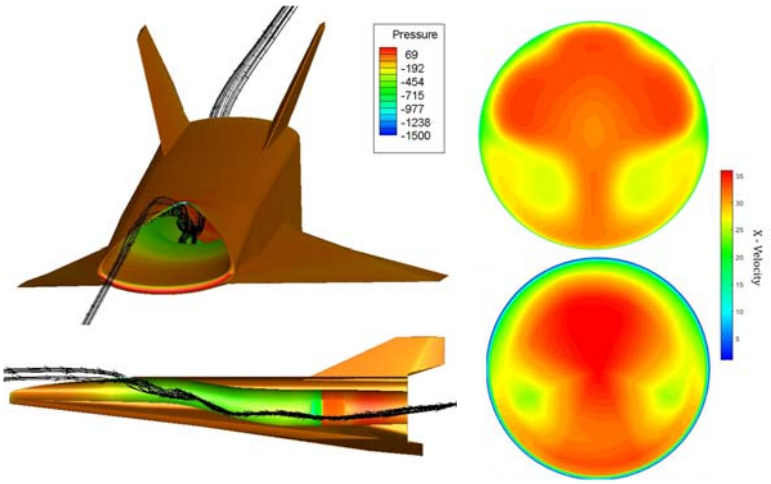

Fig 29. Vortex Flow Visualisation at 0AoA and 20A 8S Lipo at 20m/s Top Left: CFD Results (View from Front), Top Right: CFD Results at Duct Slice 0.05m Upstream of Fan, Bottom Left: CFD Results (Symmetry Plane Cross Sectional View) and Bottom Right: Wind Tunnel Results at Duct Slice 0.05m Upstream of Fan

Using tuft flow visualisation, the intake lip was also found to be prone to separation, which may also contribute to the inlet distortion. Inlet separation begins to occur and 5 degrees AoA and is severe at 15 degrees AoA. However, at a calculated take-off AoA of 8 degrees, this severe separation should never play a role in the vehicle performance. Fig. 30 below shows the separation tendencies at these critical AoAs for the take-off condition. It is important to note that the separation at the lip did not seem to be affected by forward speed or fan power setting, so the images below are indicative for all forward speeds and fan settings tested.

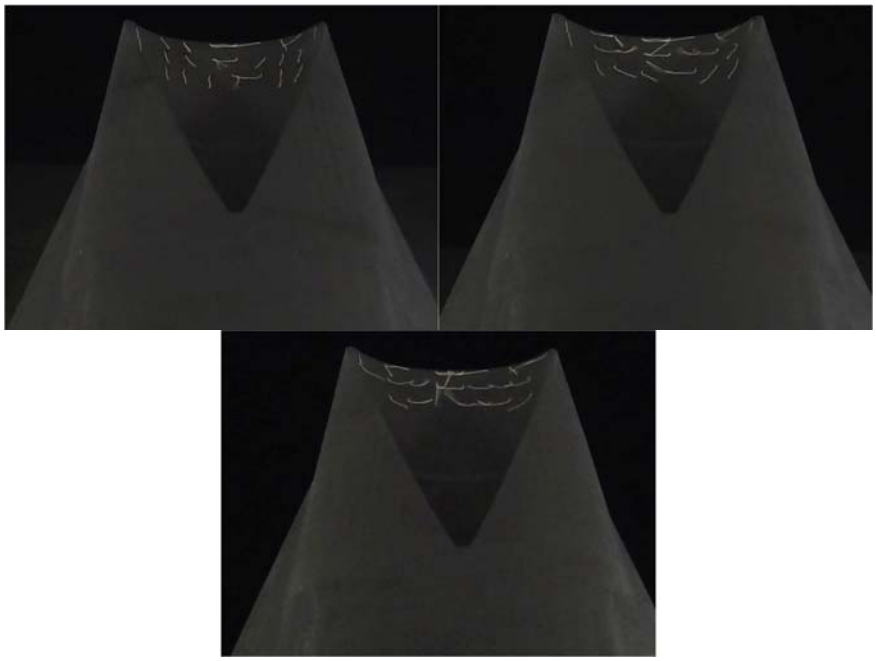

Fig 30. Tuft Flow Visualisation at Top Left: 5AoA, Top Right: 10 AoA and Bottom: 15AoA for V = 15m/s and A = 20A for 8S Lipo

4.6. Take-Off/Landing/Cruise Performance

This section will analyse the data presented in previous sections in terms of flying performance at cruise as well as take-off and landing. Fig. 31 shows the drag force variance with increasing airspeed based

on the aircraft properties presented in Table 1. A cruise speed is selected to keep AoA below 5 degrees while being speed stable. At a cruise speed of 22 m/s, the required AoA is only 3.5 degrees.

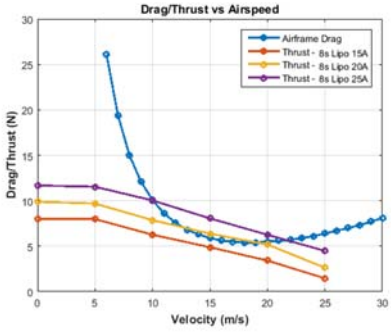

Fig 31. Thrust/Drag vs Airspeed for Cruise Configuration

A take-off speed of 15 m/s is calculated assuming the aircraft will rotate to 10 degrees AoA. The landing speed could be lowered further to 12.5 m/s if an AoA of 15 is considered. Table 4 shows a summary of these proposed landing and take-off AoAs with the achievable climb/descent rates for each fan power setting. Thrust has been recalculated based on the constant drag method for the relevant AoA. Descent rates are too high for the 15 degree AoA case for the tested fan powers, but sensible climb/descent performance is seen at the 8 degrees AoA. With increased power, better climb/descent rates are possible, but would either severely impact the flight time (less battery power left for testing) or vehicle mass (more battery power required for high AoA take-off/landing).

Table 4. Climb and Descent Rates for Two AoAs and Various Fan Power Settings with 8S Lipo Batteries

Climb/Descent Rates (m/s)					
	Fan Current Setting				
Climb/Approach AoA	5A	10A	15A	20A	25A
8 Degrees	-2.75	-0.95	0.26	1.38	2.70
15 Degrees	-8.28	-7.13	-6.85	-4.90	-3.80

5. Conclusion

Preparations for a low speed flight test program of the Hexafly-International vehicle are well underway. Modifications to the airframe included rounding of the lower intake lip and an s-bend internal duct to house a 90mm electric ducted fan have been made. An in depth wind tunnel study of the low speed variant has been completed with results from CFD simulations used to supplement the data obtained experimentally.

The vehicle aerodynamics are dominated by flow separation and vortices developing due to the sharp highly swept delta wing planform. The maximum lift to drag ratio is 4, which is very low when comparing to traditional commercial aircraft, but is expected given the geometry. Non-linear lift has been identified and help achieve a feasible take-off speed of 15m/s at and AoA of 8 degrees. Landing speeds could be further lowered to 12.5m/s should the AoA be increased to 15 degrees. A cruise speed is selected at 22m/s and the vehicle can be trimmed in this case with approximately 4 degrees elevon deflection. To maintain this cruise speed, and 8S Lipo battery pack providing 25A of current is required.

Longitudinally, the vehicle is stable up to approximately 20 degrees AoA, where an unstable pitch break occurs, but this is outside of the expected operating envelope and is not deemed a concern. Laterally, the vehicle is unstable between -5 and -2 degrees AoA, but demonstrates stable tendencies at AoAs above this. Directional stability is seen throughout the whole testing range. Asymmetric elevon deflections don't have a significant impact on the rolling moment coefficient for the range of deflections tested (up to -10/10 degrees) and further work will be required to determine solutions to this. Rudder deflections appear to be most effective at low angles of attack, after which the body of the vehicle seems to block the fins and has an adverse effect on the directional control.

The inlet performance is compromised by the unique shape of the inlet, most notably the thin upper lips where a vortex forms and is ingested by the fan. This vortex was seen in both experiments and CFD, but the fan's ability to produce the required thrust is not compromised. Tuft flow visualisation showed flow separation beginning at 5 degrees AoA and becoming more severe up to 15 degrees AoA. Static pressure measurements both up and downstream of the fan at all AoAs didn't show any significant impact of this separation, with the static pressure jump not changing significantly.

Overall, these results indicate that proceeding to the flight test phase is feasible. Some future work would need to look further into lateral and directional control in terms of achievable rotation rates as well as dynamic stability. Different mounting methods in the wind tunnel will also be investigated to remove the impact of external mounts on drag measurements.

6. References

[1] Hahne, D (1997). Evaluation of the Low-Speed Stability and Control Characteristics of a Mach 5.5 Waverider Concept. Virginia: NASA.

[2] Benoleil, A. (1994). Aerodynamic pitch-up of cranked arrow wings estimation, trim, and configuration design. Virginia: Virginia Polytechnic Institute & State University.

[3] Verhaagen N. G. and Maseland J. E. J. Investigation of the vortex flow over a 76/60° double delta wing at 20 ° incidence. AIAA-91-3208-CP, pp.70-80, 1991.

[4] McClinton, C. (2006). X-43 - Scramjet Power Breaks the Hypersonic Barrier. 44th AIAA Aerospace Sciences Meeting and Exhibit.

[5] Gibson, C., Neidhoefer, J., Cooper, S., Carlton, L. & Cox, C. (2002). Development and flight test of the X-43A-LS hypersonic configuration UAV. AIAA's 1st Technical Conference and Workshop on Unmanned Aerospace Vehicles.

[6] Gibson, C., Vess, R. & Pegg, R. (2003). Low speed flight testing of a X-43A hypersonic lifting body configuration. 12th AIAA International Space Planes and Hypersonic Systems and Technologies.

[7] Roskam, J (2007). Airplane Flight Dynamics and Automatic Flight Controls Part 1. USA: DARCorporation